High resolution characterization of modifications in fused silica after exposure to low fluence 355 nm laser at different repetition frequencies

C. H. Li,[1,2] X. Ju,[1,*] X. D. Jiang,[2] J. Huang,[2] X. D. Zhou,[2] Z. Zheng,[2] W. D. Wu,[2] W. G. Zheng,[2] Z. X. Li,[3] B. Y. Wang,[3] and X. H. Yu[4]

[1]*Department of Physics, University of Science and Technology Beijing, Beijing 100083, China*
[2]*Research Center of Laser Fusion, CAEP, P. O. Box 919-988, Mianyang 621900, China*
[3]*Institute of High Energy Physics, Chinese Academy of Sciences, Beijing 100049, China*
[4]*Shanghai Synchrotron Radiation Facility, Shanghai 201800, China*
**jux@ustb.edu.cn*

Abstract: We report on the characterization of modifications in fused silica after exposure to low fluence (2 J/cm^2) 355 nm laser at repetition frequencies of 1 Hz, 5 Hz and 10 Hz. Synchrotron based XRF spectroscopy is employed to study concentration variation of metal inclusions in the surface layer. Positron annihilation lifetime spectroscopy is used to probe atomic size defects variation in bulk silica. FT-IR is used to characterize changes of bond length and angle of Si-O-Si covalent bond of irradiated silica. Compared to the basic frequency, the big loss of cerium and iron concentration, the size enlargement of vacancy cluster and the decrease of Si-O-Si covalent bond length after 10 Hz laser irradiation are illustrated by our data. These tiny modifications provide important data to investigate laser damage mechanism.

OCIS codes: (140.3330) Laser damage; (160.6030) Silica.

References and links

1. C. Seife, and D. Malakoff, "PHYSICS: Will Livermore Laser Ever Burn Brightly?" Science **289**(5482), 1126–1129 (2000).
2. M. L. Andre, "Status of the LMJ project," Proc. SPIE **3047**, 38-42 (1996).
3. W. H. Lowdermilk, "Status of the National Ignition Facility project," Proc. SPIE **3047**, 16–37 (1996).
4. R. A. Negres, M. D. Feit, and S. G. Demos, "Dynamics of material modifications following laser-breakdown in bulk fused silica," Opt. Express **18**(10), 10642–10649 (2010).
5. A. Salleo, S. T. Taylor, M. C. Martin, W. R. Panero, R. Jeanloz, T. Sands, and F. Y. Génin, "Laser-driven formation of a high-pressure phase in amorphous silica," Nat. Mater. **2**(12), 796–800 (2003).
6. J. Wong, J. L. Ferriera, E. F. Lindsey, D. L. Haupt, I. D. Hutcheon, and J. H. Kinney, "Morphology and microstructure in fused silica induced by high fluence ultraviolet 3ω (355 nm) laser pulses," J. Non-Cryst. Solids **352**(3), 255–272 (2006).
7. R. A. Negres, M. A. Norton, D. A. Cross, and C. W. Carr, "Growth behavior of laser-induced damage on fused silica optics under UV, ns laser irradiation," Opt. Express **18**(19), 19966–19976 (2010).
8. R. A. Negres, M. W. Burke, S. B. Sutton, P. DeMange, M. D. Feit, and S. G. Demos, "Evaluation of UV absorption coefficient in laser-modified fused silica," Appl. Phys. Lett. **90**(6), 061115 (2007).
9. I. M. Burakov, N. M. Bulgakova, R. Stoian, A. Mermillod-Blondin, E. Audouard, A. Rosenfeld, A. Husakou, and I. V. Hertel, "Spatial distribution of refractive index variations induced in bulk fused silica by single ultrashort and short laser pulses," J. Appl. Phys. **101**(4), 043506 (2007).
10. K. Awazu, and H. Kawazoe, "Strained Si–O–Si bonds in amorphous SiO_2 materials: A family member of active centers in radio, photo, and chemical responses," J. Appl. Phys. **94**(10), 6243–6262 (2003).
11. J. Neauport, L. Lamaignere, H. Bercegol, F. Pilon, and J. C. Birolleau, "Polishing-induced contamination of fused silica optics and laser induced damage density at 351 nm," Opt. Express **13**(25), 10163–10171 (2005).
12. C. H. Li, X. Ju, W. D. Wu, X. D. Jiang, J. Huang, W. G. Zheng, and X. H. Yu, "Synchrotron micro-XRF study of metal inclusions distribution and variation in fused silica induced by ultraviolet laser pulses," Nucl. Instrum Meth. B **268**(9), 1502–1507 (2010).
13. M. F. Guerra, M. Radtke, I. Reiche, H. Riesemeier, and E. Strub, "Analysis of trace elements in gold alloys by SR-XRF at high energy at the BAMline," Nucl. Instrum Meth. B **266**(10), 2334–2338 (2008).

#136746 - $15.00 USD Received 28 Oct 2010; revised 15 Dec 2010; accepted 5 Jan 2011; published 22 Mar 2011

14. L. Vincze, B. Vekemans, F. E. Brenker, G. Falkenberg, K. Rickers, A. Somogyi, M. Kersten, and F. Adams, "Three-dimensional trace element analysis by confocal X-ray microfluorescence imaging," Anal. Chem. **76**(22), 6786–6791 (2004).
15. S. Ghosh, P. M. G. Nambissan, and R. Bhattacharya, "Positron annihilation and Mössbauer spectroscopic studies of In^{3+} substitution effects in bulk and nanocrystalline $MgMn_{0.1}Fe_{1.9-x}In_xO_4$," Phys. Lett. A **325**(3-4), 301–308 (2004).
16. M. R. Kozlowski, J. Carr, I. Hutcheon, R. Torres, L. Sheehan, D. Camp, and M. Yan, "Depth profiling of polishing-induced contamination on fused silica surface," Proc. SPIE **3244**, 365–375 (1998).
17. H. Hosono, Y. Ikuta, T. Kinoshita, K. Kajihara, and M. Hirano, "Physical disorder and optical properties in the vaccum ultraviolet region of amorphous SiO_2," Phys. Rev. Lett. **87**(17), 175501 (2001).
18. J. C. Conde, F. Lusquinos, P. Gonzalez, B. Leon, and M. Perez-Amor, "Temperature distribution in a material heated by laser radiation: modeling and application," Vacuum **64**(3-4), 359–366 (2002).

1. Introduction

Fused silica is an increasingly important material in modern high tech industries [1], a prominent example being bulk material as transparency optics for large high power output systems such as Laser Megajoule and National Ignition Facility [2,3]. In these applications, to avoid optical breakdown, material stability under laser irradiation is a key requirement [4,5]. Previous studies have shown that significant damage in the form of craters can be produced in fused silica optics under high fluence laser irradiation [6]. The lateral size of this damage grows exponentially with the number of pulses and reduces the lifetime of the optics [7].

However, relatively low laser fluence but large number of shots and high repetition frequency is the most commonly used situation for fused silica optics. Low fluence laser induced transmission loss, unacceptable refractive index change and surface roughing in fused silica are revealed by recent studies [8,9]. Besides, characterization of material modifications induced by low fluence laser provides a physical basis for understanding the laser damage mechanism. In this paper, we attempt to characterize the tiny modifications in fused silica induced by low fluence laser at different repetition frequencies. Based on the X-ray and neutron scattering results, the fused silica can be considered as a continuous network consisting of relatively rigid, undistorted $Si(O_{1/2})_4$ tetrahedron, connected at corners by shared (bridging) oxygen atoms [10]. Radiation-induced defects formation and variation can be involved with the distortion of the $Si(O_{1/2})_4$ tetrahedron, the fracture of Si-O-Si covalent bond, and the diffusion and rearrangement process of formed defects. Despite polishing-induced contamination being widely accepted as laser energy absorption source [11,12], the concentration variation of surface metals under laser irradiation is of significant meaning to understand initiation of laser energy absorption.

To characterize the variation of very low concentration of surface metal inclusions with high resolution, the synchrotron based X-ray fluorescence (SXRF) microprobe is employed. XRF is one of the most widely used spectroscopic techniques in elemental identification and quantification [13]. When using synchrotron sources to produce the exciting micro-beam, taking advantages of the high intensity, natural collimation, potential tunability, and high degree of linear polarization in the storage ring plane, these advantages offer the possibility to obtain high elemental and chemical sensitivity with trace level detection limits [14]. To characterize the tiny variation of atomic size vacancy defects with high detection sensitivity, the positron annihilation lifetime spectroscopy (PALS) probe is used. Due to the relatively small diameter (0.106 nm) of the o-Ps formed in process of positron interaction with surfaces, the PALS probe have advantages of being in situ, non-invasive and non-comparable sensitive compared to other methods. The obtained systematic data are used to clarify the possible relationship between the concentration variation of surface metal inclusions and a series of related modifications in fused silica such as variation of atomic size vacancy defects and variation of bond angle and length of Si-O-Si covalent bond and to acquire physical insight into the laser damage process.

#136746 - $15.00 USD Received 28 Oct 2010; revised 15 Dec 2010; accepted 5 Jan 2011; published 22 Mar 2011

2. Experimental

2.1 Samples and UV laser irradiation

The substrates used for the experiments were UV-grade Corning 7980 fused silica which was manufactured by flame hydrolysis and contained 800-1000 ppm by weight of OH. The fused silica samples with a dimension of 10 × 10 × 1 mm^3 were optically polished on both surfaces using best-known continuous pitch polishing techniques. Ceria was chosen as polishing powder. Prior to laser irradiation, all samples have been washed thoroughly with distilled de-ionized water to rinse off any particles induced by storage and handling on the optic surface, which was followed by an alcohol rinse with absolute ethanol to remove residual water. The samples were then air dried in a laminar hood. During the manufacturing process, some metal elements were inevitably introduced in the surface layer of optics. For instance, iron and nickel were introduced by sawing and cutting tools, copper and zinc were caused by grinding disc, and cerium was originated from the using of ceria as polishing powders [11]. However, these contaminants cannot be easily removed by the above cleaning procedure. A frequency tripled Nd-YAG laser was employed at ambient conditions in this experiment. The wavelength was 355 nm and the pulse length (full width at half maximum, FWHM) was ~6.8 ns. The examined repetition frequencies in this study were 1 Hz, 5 Hz and 10 Hz, and the irradiated laser pulses number was uniformly set as 100. The energy of each pulse was measured by a calorimeter. The actual measured average laser fluence of 100 laser shots was 2 J/cm^2 with an energy deviation less than 3%. The beam temporal and spatial profile was both near Gaussian with a $1/e^2$ diameter of 0.4 mm at the sample plane. The raster scan mode was used to secure the irradiated region larger than 8 × 8 mm^2 on the silica surface.

2.2 Synchrotron induced X-ray fluorescence spectroscopy

Synchrotron induced X-ray fluorescence spectroscopy was carried out at the BL15U1 beam line of SSRF (Shanghai Synchrotron Radiation Facility). SSRF is a third generation synchrotron radiation facility with operating at an electron energy of 3.5 GeV and an injection current of ~210 mA. The synchrotron white beam emerging from the bending magnet source was monochromatized with a double-crystal Si (111) monochromator. The energy of the emerging photon beam can be tuned within the range of 3.5 keV and 22.5 keV. The cross sectional area of the beam can also be adjusted by a pair of Kirkpatrick-Baez mirrors systems. To provide the maximum achievable flux at the sample position and ensure the interest metals can be excited, the excitation photon energy selected in this study was 10 keV and beam dimensions were set as 100 μm × 100 μm, with photon flux available was ~1.7×10^{11} photons/s/mm^2. The characteristic X-rays fluorescence signal and the signals needed for normalization, e.g. ionization chamber signals, detector dead time and ring current, were detected with a liquid nitrogen cooled energy dispersive Si(Li)-based detection system. To provide significant suppression of the scattered photon intensity, the 90° geometrical arrangement between the incident synchrotron beam and the detector was arranged. The signal collection time for each point was set as 120 s.

The acquired spectra were analyzed using the software WinAxil developed for spectroscopy. The spectra were smoothed using a procedure based on de-convolution, leading to the removal of peak broadening effects caused by the imperfect resolution of the measuring instruments. The spectra were subsequently fitted using a procedure based on the Levenburg-Marquardt non-linear minimization algorithm. The fitting process took into account a linear baseline resulting in an estimation of the net total of counts integrated over the width of the photopeak.

2.3 Positron annihilation lifetime spectroscopy

The PALS spectra were measured with a slow–fast coincidence system. Two identical samples were placed on each side of a ^{22}NaCl positron source of activity about 17.8×10^5 Bq, deposited on a pure Mylar film. The resolving time (FWHM) of this experimental system, measured for prompt gamma rays from ^{60}Co source was 189 ps at the positron window

#136746 - $15.00 USD Received 28 Oct 2010; revised 15 Dec 2010; accepted 5 Jan 2011; published 22 Mar 2011

settings, with a time constant of 55 ps/channel in the multi-channel analyzer. All lifetime measurements were performed at room temperature and a total of ~2 × 10^6 counts were collected over a period of 4 hours. The measured positron lifetimes spectra were analyzed using the LT 9.0 program. All the lifetime spectra were best fitted by three lifetime components with free intensity and lifetime. The fitting errors in measuring the lifetime correspond to a standard deviation of ~1%. By considering the contribution of Mylar in the positron source to PALS spectra, an additional source component with fixed lifetime (385 ps) and intensity (13%) was subtracted during data analysis.

Two longer lifetime components were the parameters that indicate information of vacancy defects, with lifetime representing the relative size of annihilation pores and the intensity representing the relative concentration of pores. Using a well-developed formalism for two-state positron trapping model [15], the following parameters can be calculated according to Eq. (1):

$$\tau_b = \frac{I_1 + I_2}{I_1/\tau_1 + I_2/\tau_2}, \quad \tau_{av} = \frac{\tau_1 I_1 + \tau_2 I_2}{I_1 + I_2}, \quad k_d = \frac{I_2}{I_1}\left(\frac{1}{\tau_b} - \frac{1}{\tau_2}\right) \tag{1}$$

where τ_b – positron lifetime in defect-free bulk, $\tau_{av.}$ – average positron lifetime, k_d – positron trapping rate of defect. In addition, the difference $\tau_2 - \tau_b$ can be accepted as a size measure of extended defects, as well as the ratio τ_2/τ_b represents the nature of these defects.

2.4 FT-IR and AFM

Fourier transform infrared absorption spectra were obtained by a Nicolet 5700 spectrometer. A reflection mode was employed to measure the FT-IR absorption spectra in the frequency region associated with the Si–O–Si stretching and bending vibrations, ranging 400–1600 cm^{-1}. The spectral resolution was 1.9285 cm^{-1}. AFM images were collected by a Benyuan CSPM 5000 system. The highest obtained resolution of this AFM was 0.26 nm in surface plane. The scanning area was 20 × 20 μm^2 square.

2.5 Statistical consideration

To verify the data reproducibility and ensure the observed modifications is common in samples other than just an isolated result in this experiment; the parallel samples method was employed. Specifically, three parallel samples were prepared and irradiated by UV laser pulses with same parameters. These three parallel samples were tested by SXRF, PALS, IR and AFM methods with same conditions. For example, Fig. 1 shows SXRF spectra for three parallel samples irradiated by 355 nm laser at different frequencies. The reproducibility of PALS, IR and AFM data were also examined during our actual measurements. For the sake of concise, the illustration figures were not presented. The data reproducibility can be ensured since the obtained data show fairly congruence. On the other hand, to ensure the statistical meaning of the obtained data, the SXRF spectra for five randomly selected isolated points in the irradiated zone were collected. The acquired five SXRF spectra show good consistency and the average spectrum was used for discussion. For PALS, IR and AFM measurements, a relatively big sampling area was selected to ensure the observed modifications reflect statistical information of large region in optics.

#136746 - $15.00 USD Received 28 Oct 2010; revised 15 Dec 2010; accepted 5 Jan 2011; published 22 Mar 2011

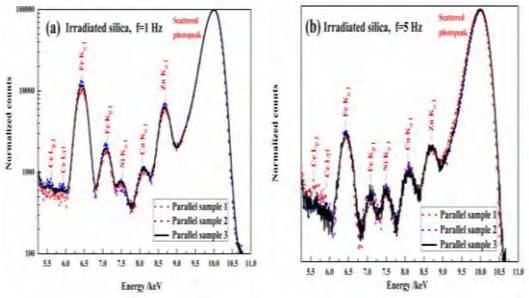

Fig. 1. SXRF spectra obtained for three parallel samples irradiated by UV laser with same parameters (F = 2 J/cm^2, 100 pulses).

3. Results

3.1 Surface metal concentration variation

Figure 2 shows comparisons between the spectrum of pristine silica surface and the spectra resulting from the laser irradiated zone. Characteristic peaks for cerium, iron, nickel, copper and zinc are clearly presented in the spectrum for pristine silica surface. The variation of cerium, iron, nickel and copper are examined in detail because of these metals are likely to lead to strong absorption in the UV region [16]. The variation of metal concentration can be revealed by the normalized peak area of characteristic photopeaks to some extent.

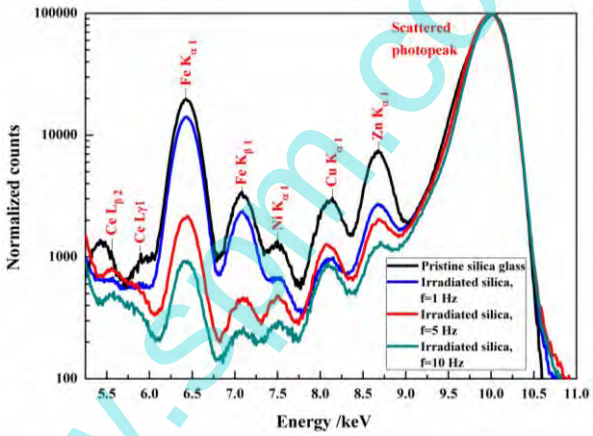

Fig. 2. SXRF spectra obtained both for pristine silica surface and irradiated zone.

Figure 3 shows the variation of normalized peak areas for cerium, iron, nickel and copper versus repetition frequency. The normalized peak areas show an exponentially decreasing trend as the linearly elevation of repetition frequency. The obtained decrement of normalized peak areas for cerium, iron, nickel and copper are 81.6%, 93.5%, 74.1% and 64.3%, respectively. It is worthwhile to point out that the obtained decrement for cerium and iron are the biggest. This result is in accordance with the fact that iron and cerium ions have the biggest absorption cross section of about 8×10^{-19} cm^2. This large removal of metals indicates that sufficient laser energy is absorbed in the thin surface layer.

#136746 - $15.00 USD Received 28 Oct 2010; revised 15 Dec 2010; accepted 5 Jan 2011; published 22 Mar 2011

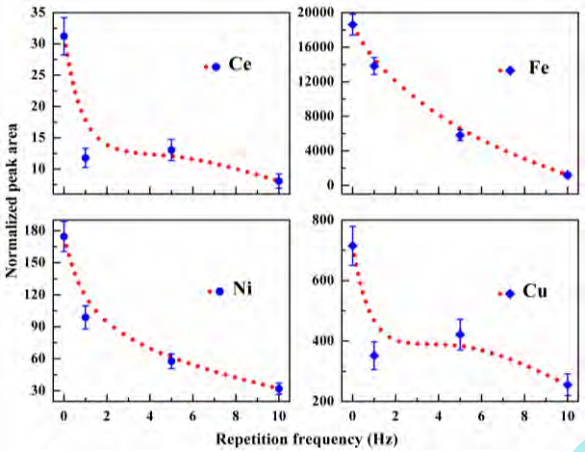

Fig. 3. Semi-quantitative analysis for cerium, iron, nickel and copper variation under elevating repetition frequency laser irradiation. Red dot lines were used to aid the eyes.

3.2 Vacancy defects variation

Table 1 lists the measured PALS parameters for the examined samples. The short lifetime component τ_1 of about 144 ps describes free positron annihilated in Si-O-Si network structure. The second lifetime τ_2 (0.768 ns) can be associated with the trapping of positrons in mono-vacancies, vacancy clusters and small cavities. The third lifetime τ_3 at the level of 1.5~1.65 ns is due to "pick-off" annihilation of o-Ps atoms in structural pores between discontinued $Si(O_{1/2})_4$ tetrahedron network structure. As can be seen from Table 1, the measured lifetime components obviously differ for untreated and irradiated samples. The longer τ_2 and τ_3 lifetimes with greater I_2 but smaller I_3 intensity characterize the laser irradiated samples. Respectively, the laser irradiated samples possess longer average τ_{av} and bulk τ_b, as well as larger value of $\tau_2 - \tau_b$.

Table 1. Effect of repetition frequency on the PALS parameters for fused silica (F = 2 J/cm^2; 100 pulses)

Irradiation	Lifetime components						Positron trapping modes				
Frequency Hz	τ_1	τ_2	τ_3	I_1	I_2	I_3	τ_{av}	τ_b	k_d	$\tau_2-\tau_b$	τ_2/τ_b
		ns			%		ns		ns^{-1}	ns	
0	0.144	0.768	1.591	34.9	19.4	45.7	0.367	0.204	2.00	0.560	3.77
1	0.144	0.769	1.598	35.3	19.7	45	0.368	0.204	2.02	0.565	3.78
5	0.144	0.792	1.606	35.9	21.1	43	0.384	0.207	2.10	0.585	3.83
10	0.148	0.812	1.628	36.5	21.4	42.1	0.393	0.212	2.05	0.600	3.84

As is displayed in Fig. 4, the value of τ_2 increases from 0.768 ns to 0.812 ns with a 5.7% increase as repetition frequency elevates to 10 Hz. An elevation of 10.3% in intensity I_2 is also observed. The increase of τ_2 and $\tau_2 - \tau_b$ both suggest that the size of vacancy cluster is enlarged after irradiation. The value of τ_3 increases from 1.591 ns to 1.628 ns obtaining only a 2.3% increase, while the intensity of I_3 obtains a 7.8% decrease. The proportion of vacancy cluster increases by 10.3% revealing that part of Si-O-Si covalent bond is fractured under laser irradiation.

#136746 - $15.00 USD Received 28 Oct 2010; revised 15 Dec 2010; accepted 5 Jan 2011; published 22 Mar 2011

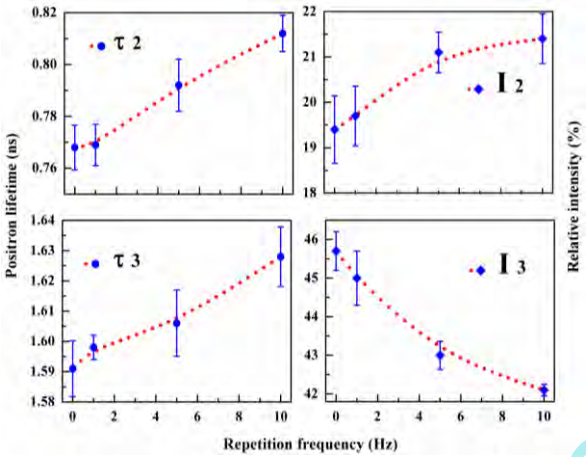

Fig. 4. Deconvoluted PALS lifetime and intensity under different repetition frequencies laser irradiation. Red dot lines were used to aid the eyes.

3.3 Structural modification

Figure 5 reveals the presence of two transverse optical modes (TO) of the Si–O–Si groups: the bending Si–O–Si vibration identified around 800 cm^{-1}, and the asymmetric stretching (AS) mode Si–O–Si located around 1050 cm^{-1}. Figure 5 also presents a gradually intensity attenuation trend of both the oxygen bending mode and the AS mode of Si–O–Si vibration with the elevation of repetition frequency. Figure 6(a) presents the deconvoluted IR spectrum for laser irradiated silica surface at f = 10 Hz. The spectrum is deconvoluted by Gauss function with a Shirley baseline subtraction using a standard χ^2 minimization procedure. The deconvolution procedure is based on the fact that the Si–O–Si AS mode can be split into the longitudinal optical mode (LO, ~1033 cm^{-1}) for octahedral SiO_2 and transverse optical mode (TO, ~1076 cm^{-1}) for tetrahedral SiO_2 [5]. This splitting phenomenon is also observed for SiO_x films as *x* decrease from two [17].

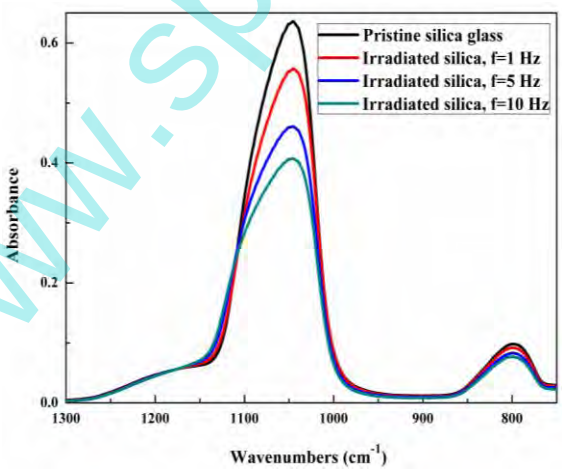

Fig. 5. FT-IR spectra obtained both for pristine silica surface and irradiated zone.

Figure 6(b) gives the statistic peak area variation versus repetition frequency. The proportion of statistic peak area of LO mode (~1033 cm^{-1}) gains an exponentially decreasing trend while the opposite trend is obtained for TO mode (~1076 cm^{-1}). The proportion of TO

#136746 - $15.00 USD Received 28 Oct 2010; revised 15 Dec 2010; accepted 5 Jan 2011; published 22 Mar 2011

mode (~1076 cm^{-1}) increases by 28% as the repetition frequency elevates to 10 Hz. This result discloses the fact that the contribution of higher frequency vibration is increased as the repetition frequency is elevated. Based on the central force model, the decreasing length of Si-O-Si covalent bond and increasing Si-O-Si bond angle are responsible for the vibration mode shift to higher frequency. The decrease of Si-O-Si bond length also reflects that the modified material is densified. The FT-IR results combines PALS results completely illustrates structural modifications in fused silica under laser irradiation.

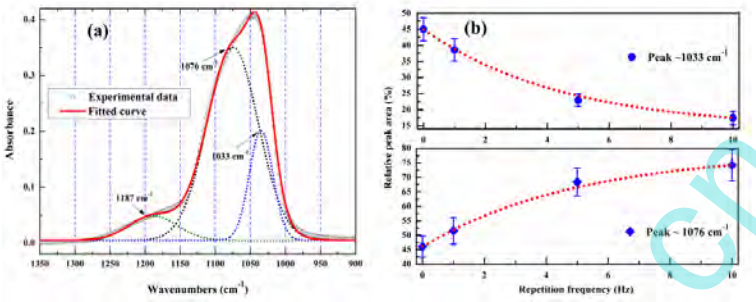

Fig. 6. The deconvoluted IR spectrum (a) and semi-quantitative analysis for peak area variation under elevating repetition frequency laser irradiation (b). Red dot lines were used to aid the eyes.

3.4 Surface morphology modification

Figure 7(b)–7(d) show that sub-micron scale voids located on the surface of laser irradiated silica glass. Figure 7(a) shows that such voids are absent in the pristine silica glass surface. To estimate the size of those voids, 50 largest well-defined voids are selected and measured. For samples irradiated by laser pulses at f = 1 Hz, 5 Hz and 10 Hz, the calculated mean value and standard deviation for void diameter is 110 ± 12 nm, 190 ± 38 nm, and 260 ± 50 nm, respectively. At low repetition frequency of 1 Hz, a few discrete voids along the preexisting scratches are observed. As repetition frequency elevates from 1 Hz to 10 Hz, voids size enlarges and voids number increases and the void shape becomes rather arbitrary. Besides, voids formed by 5 Hz and 10 Hz laser irradiation are more randomly dispersed on the irradiated zone than localized along the preexisting scratches. Besides, the average roughness (S_a) value of these examined area is increased from 0.54 nm to 0.95 nm. The depth of these voids is not easy to exactly determined, but most of them can be qualitatively estimated to be less than 8.5 nm. This suggests that the morphology alteration is localized in surface layer.

#136746 - $15.00 USD Received 28 Oct 2010; revised 15 Dec 2010; accepted 5 Jan 2011; published 22 Mar 2011

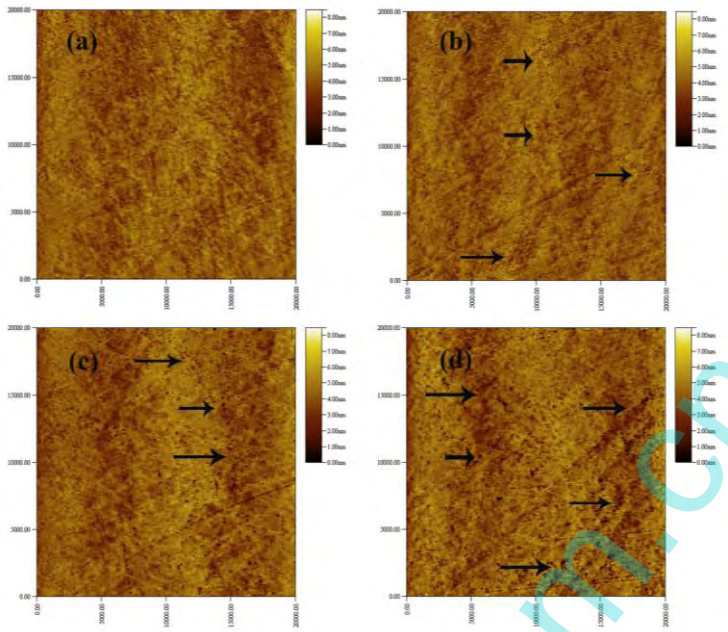

Fig. 7. AFM images of typical surface morphology both for untreated and laser irradiated samples, (a) Pristine silica surface; (b) f = 1 Hz; (c) f = 5 Hz; (d) f = 10 Hz. The scanning area is 20 × 20 μm^2. Black arrows pointing to some typical voids are added to aid the eyes.

4. Discussion

4.1 Effect of repetition frequency

Figure 2 and 3 present that the effect of repetition frequency on metal concentration is significant. As repetition frequency elevated from 1 Hz to 10 Hz, the obtained decrement of normalized peak area for cerium, iron, nickel and copper is 12%, 68%, 25.8% and 32.1%, respectively. This result suggests that the four interested metals all actively involved in laser energy absorption process under high repetition frequency laser irradiation. Because of the decrement of iron is the biggest (68%), we can infer that the absorption coefficient of iron must be experienced a steep rise under high repetition frequency laser irradiation. Correspondingly, the effects of repetition frequency on vacancy defects variation, structural and morphological modification are revealed by PALS spectra, IR and AFM images, as depicted by Figs. 4–7.

According to the numerical calculation results of heat transfer after laser irradiation, which is based on the conventional Fourier thermal conduction theory, the integrated heat during pulse duration of ~20 ns can be estimated to be dissipated almost thoroughly within 200 ns [18]. Therefore, the thermal integration induced by laser pulse with 6.8 ns width in our experiment at different repetition frequencies in the range of 1~10 Hz can be neglected.

The —material response delay" was suggested to be responsible for the observed difference in modification as a function of repetition frequency. The time delay of material response in bulk fused silica following localized energy deposition via laser-induced breakdown is greatly longer than the process of heat transfer. R. A. Negres, et al. established an effective time-resolved imaging system to monitor the material response such as the propagation of shock waves, near-surface material motion, the speed of ejecta and material transformations following laser energy deposition [4]. Experimental results indicate that the material response can be separated into distinct phases, some terminating within a few tens of nanosecond but some processes such as the returning of melted regions to solid phase extending up to about 100 ms order (pump laser, 355 nm, 7 ns). For 10 Hz laser irradiation, the cooling period for

#136746 - $15.00 USD Received 28 Oct 2010; revised 15 Dec 2010; accepted 5 Jan 2011; published 22 Mar 2011

each shot is about 100 ms, which indicates that before the laser modified material returns to normally solid phase, the successive laser shots will be released. Due to the higher absorption coefficient of modified material, the ongoing interaction between successive laser shots and the incompletely recovered material for 10 Hz and 5 Hz laser will be stronger than that for 1 Hz laser irradiation.

The modification of temporal and spatial profile of laser beams at different frequencies is suggested as another origination. Since the examined temporal profiles at different frequencies show no difference, the modification of temporal profiles can be neglected. However, as is depicted by Fig. 8, there exists difference in spatial distribution of laser beams at different repetition frequencies. The calculated effective area for 1 Hz, 5 Hz and 10 Hz laser beams is 0.452 mm^2, 0.489 mm^2, 0.478 mm^2, respectively. The peak to average intensity ratio for 1 Hz, 5 Hz and 10 Hz laser beams is 2.66, 2.80, and 2.88, respectively. Besides, the area of strong intensity zone (orange color zone in Fig. 8) is increased as the elevating of repetition frequency. Correspondingly, the ratio of strong intensity zone area to the beam's effective area is increased from 0.42% (1 Hz) to 3.52% (10 Hz). This indicates that laser energy on the sample plane assume more localized distribution for higher repetition frequency. Thus, the actual laser fluence in small strong intensity zone on the optics at 10 Hz and 5 Hz laser irradiation will be higher than that of basic frequency.

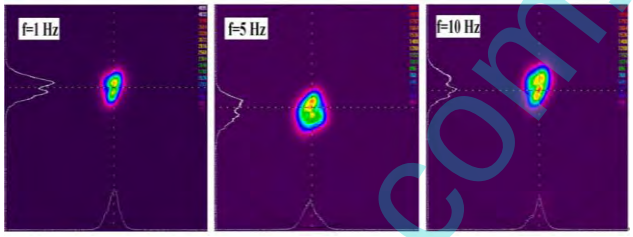

Fig. 8. The spatial distribution of laser beams at different repetition frequencies.

4.2 Damage process

Local metal inclusions initiate laser energy absorption through avalanche process and multi-photon absorption process. Once sufficient laser energy is absorbed, the steep temperature rise of metal inclusion is easily obtained, and boiling, evaporation, and explosion of metal inclusion will occur. Therefore, the decreasing of metal concentration revealed in Fig. 2 and 3 reflects the energy absorption process. When low laser fluence irradiates on the silica, it undergoes explosion of metal inclusion and the subsequent ejection of bulk silica. As a result, surface morphology modifications such as voids and cracks form, as depicted by Fig. 7. Furthermore, shock waves generated by phase explosion will further compress the $Si(O_{1/2})_4$ tetrahedron. The decrease of Si-O-Si covalent bond length and densification of surrounding bulk silica phenomenon is clearly depicted by Fig. 5 and 6. PALS results reflects what has happened in bulk silica after the Si-O-Si covalent bond is compressed and even fractured, as depicted in Fig. 4. In short, metal inclusions initiate energy absorption, and the localized energy of metal inclusions is gradually dissipated in bulk silica through surface morphology modification and medium range structural modification and variation of vacancy defects. Therefore, strictly controlling on the concentration of metal inclusions such as cerium and iron is of particular importance for controlling laser-induced damage.

5. Conclusions

In this paper, combined methods of SXRF, PALS, FT-IR and AFM were employed to characterize the tiny modifications in fused silica after exposure to low fluence 355 nm laser at different repetition frequencies. The revealed significant decreasing of metal concentration certifies the viewpoint that metal inclusions strongly absorb incident laser energy and they themselves were vaporized and removed during laser energy absorption process. The enlarged

#136746 - $15.00 USD Received 28 Oct 2010; revised 15 Dec 2010; accepted 5 Jan 2011; published 22 Mar 2011

size and increased number of surface nano-sacle voids with elevating repetition frequency was caused by the metal inclusion vaporization and micro-explosion at surface. FT-IR results suggested that the bond length of Si-O-Si covalent was decreased and the bond angle of Si-O-Si was increased after laser irradiation. PALS results illustrated that the size of vacancy cluster was enlarged and proportion was also increased after irradiation. These results disclosed that the $Si(O_{1/2})_4$ tetrahedron was compressed, and the Si-O-Si covalent bond was fractured under laser irradiation. Due to laser intensity modulation at absorbing sites, the size and intensity variation of vacancy cluster caused significant increase of absorption cross section which in turn induces severe laser energy absorption. High repetition frequency laser irradiation introduced more severe laser energy absorption and related morphological and structural modifications than basic frequency laser irradiation. Based on the obtained systematic data, the damage process was discussed in terms of energy transfer route during laser-material interaction.

Acknowledgements

We acknowledge Dr. Hua Wang and Dr. Fen Yan at the Shanghai Synchrotron Radiation Facility for their beam line support during data collection. This work is financially supported by National HI-TECH Research and Development Program of China under Grant No. 2008AA8040508.

#136746 - $15.00 USD Received 28 Oct 2010; revised 15 Dec 2010; accepted 5 Jan 2011; published 22 Mar 2011